

Transport of surface-modified iron nanoparticle in porous media and application to arsenic(III) remediation

Sushil Raj Kanel · Dhriti Nepal · Bruce Manning · Heechul Choi

Received: 3 August 2006 / Accepted: 12 February 2007
© Springer Science+Business Media B.V. 2007

Abstract The surface-modified iron nanoparticles (S-INP) were synthesized, characterized and tested for the remediation of arsenite (As(III)), a well known toxic groundwater contaminant of concern. The S-INP material was fully dispersed in the aqueous phase with a particle size distribution of 2–10 nm estimated from high-resolution transmission electron microscopy (HR-TEM). X-ray photoelectron spectroscopy (XPS) revealed that an Fe(III) oxide surface film was present on S-INP in addition to the bulk zero-valent Fe⁰ oxidation state. Transport of S-INP through porous media packed in 10 cm length column showed particle breakthroughs of 22.1, 47.4 and 60 pore volumes in glass beads, unbaked sand, and baked sand, respectively. Un-modified INP was immobile and

aggregated on porous media surfaces in the column inlet area. Results using S-INP pretreated 10 cm sand-packed columns containing ~2 g of S-INP showed that 100 % of As(III) was removed from influent solutions (flow rate 1.8 mL min⁻¹) containing 0.2, 0.5 and 1.0 mg L⁻¹ As(III) for 9, 7 and 4 days providing 23.3, 20.7 and 10.4 L of arsenic free water, respectively. In addition, it was found that 100% of As(III) in 0.5 mg/L solution (flow rate 1.8 mL min⁻¹) was removed by S-INP pretreated 50 cm sand packed column containing 12 g of S-INP for more than 2.5 months providing 194.4 L of arsenic free water. Field emission scanning electron microscopy (FE-SEM) showed S-INP had transformed to elongated, rod-like shaped corrosion product particles after reaction with As(III) in the presence of sand. These results suggest that S-INP has great potential to be used as a mobile, injectable reactive material for *in-situ* sandy groundwater aquifer treatment of As(III).

S. R. Kanel · H. Choi (✉)
Department of Environmental Science and Engineering, Gwangju Institute of Science and Technology (GIST), 1-Oryong-dong, Buk-gu 500-712 Gwangju, The Republic of Korea
e-mail: hcchoi@gist.ac.kr

D. Nepal
Department of Materials Science and Engineering, Gwangju Institute of Science and Technology (GIST), 1-Oryong-dong, Buk-gu 500-712 Gwangju, The Republic of Korea

B. Manning
Department of Chemistry and Biochemistry, San Francisco State University, 1600 Holloway Avenue, San Francisco, California 94132, USA

Keywords Nanoparticles · Surfactants · Arsenic · In-situ treatment · Environmental remediation

Introduction

Application of nanomaterials for environmental remediation has recently received great attention (Huber 2006; Li et al. 2006). Among the different

nanomaterials, iron nano particles (INP) have been extensively studied to remediate pollutants such as chlorinated organic compounds and metal ions (Zhang 2003; Lowry and Johnson 2004; Wang and Zhang 1997), nitrate (Choe et al. 2000), Cr(VI) and Pb (Ponder et al. 2000), carbon tetrachloride and benzoquinone (Nurmi et al. 2005), metalloids such as arsenic (Kanel et al. 2005, 2006) and organic compounds (Joo et al. 2004). Recent attention on arsenic contamination in groundwater has resulted in research on the potential use of INP as a remediation material (Kanel et al. 2005, 2006). Arsenic is one of the most toxic, naturally occurring groundwater contaminants and exists as arsenate (As(V)) oxyanions ($\text{H}_2\text{AsO}_4^{-1}$ and HAsO_4^{-2}) at neutral pH under oxidizing conditions (Ferguson 1972) and arsenite (As(III)) under mildly reducing conditions. The As(III) species remains protonated as H_3AsO_3^0 at pH below 9.2 (Ferguson 1972; Manning et al. 2002).

Recent investigations have confirmed that INP and their corrosion products are suitable materials for remediation of both As(III) and As(V) (Kanel et al. 2005, 2006; Manning et al. 2002). However, the tendency for INP to aggregate during oxidative corrosion to Fe(III) oxide/hydroxide limits the effective transport and delivery of INP through porous media, which is normally essential for in-situ groundwater remediation (Nurmi et al. 2005; O'Hena et al. 2006). As a result, surface modified INP (S-INP) has been synthesized using stabilizers such as polyacrylic acid (Schrick et al. 2004), starch (He and Zhao 2005), noble metals (Elliott and Zhang 2001) and oil (O'Hena et al. 2006; Quinn et al. 2005). Though these results show promise, the majority of these studies have focused on removal of chlorinated organic contaminants such as TCE and most have used a batch reaction approach. To the best of our knowledge, investigation of the transport of non-ionic surfactant stabilized S-INP in sand packed columns combined with tests for the removal of dissolved arsenic has never been reported.

Given the great potential for environmental remediation applications of S-INP, our objectives were to (1) synthesize and characterize the physical properties of nonionic surfactant modified S-INP, (2) determine the hydraulic transport

properties of S-INP through porous media-packed columns, and (3) investigate the application of S-INP to As(III) remediation.

Experimental Section

Chemicals and materials

The chemicals used (NaAsO_2 , HCl, NaNO_3 , NaCl, KI, and NaBH_4) were reagent grade obtained from Aldrich or Fluka Chemical Company. For column studies, glass beads, unbaked sand, baked sand (Jumunjin, South Korea) were used (Kanel et al. 2003). Glass beads were soaked in hydrogen peroxide solution for 10 h and washed with deionized (DI) water followed by baking at 105 °C for 24 h and sieved to 425–600 μm before use. Baked sand was prepared by baking at 500 °C for 24 h to eliminate organic matter sorbed on surfaces (Choi et al. 2002). The elemental composition of the sand was determined with a JEOL X-ray fluorescence (XRF) spectrometer (JSX 3201Z) (Table 1). The XRF results of the sand provided the chemical composition (expressed as the metal oxide content, % w:w) which was dominated by SiO_2 (90.32%) and Al_2O_3 (5.48%) with a small amount of Fe_2O_3 (0.12%). The loss of ignition (LOI) measured value of 0.14% (w:w) suggested a relatively low

Table 1 Chemical composition of Jumunjin sand (South Korea)

Component	(% weight)
SiO_2	90.32
Al_2O_3	5.48
Fe_2O_3^a	0.12
TiO_2	0.02
MnO_2	0.05
CaO	0.07
MgO	0.03
K_2O	3.40
Na_2O	0.36
P_2O_5	0.01
LOI ^b	0.14
Total	100.00
Organic matter content (%)	0.12

a : Total Fe

b : loss on ignition

Elemental results from X-ray fluorescence (XRF) analysis are presented as mass of the metal oxide

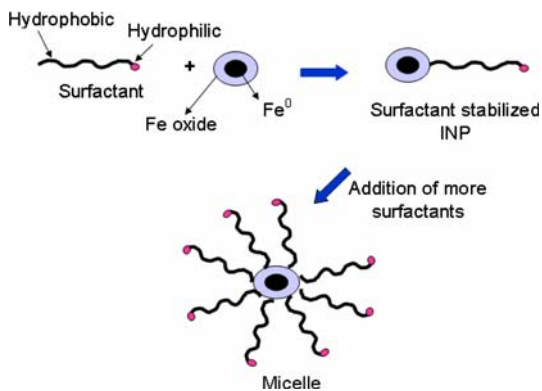
Table 2 Representative physical properties of glass beads, sand, and baked sand packed in short columns (10 cm length)

Properties	Glass Beads	Sand	Baked sand
Organic matter Content (%)	0.00	0.12	0.00
Porosity	0.39	0.58	0.51
Bulk Density (g/cm ³)	1.50	1.50	1.60
Surface area (m ² /g)	0.03	0.64	1.22
Particle Size (μm)	425–600	425–600	425–600

water and organic matter content and low surface area (Table 2). The porous media XRD patterns revealed that the sand was dominated by a quartz-like phase with characteristic peaks at 20.3, 26.1, 50.0, 60.0 degrees with additional smaller unidentified peaks whereas glass beads were amorphous (data not shown here).

Preparation of nanoparticles

Iron nano-particles were synthesized using previously reported methods with slight modification (Kanel et al. 2005, 2006). In this study 30% aqueous ethanol was used instead of 100% deionized (DI) water and no attempts were made to synthesize INP under inert atmosphere. The S-INP was prepared by dispersing 1 g/L INP particles in aqueous 0.5% Tween 20, non-ionic surfactant (polyoxyethylene sorbitan monolaurate), which is nontoxic and biodegradable, followed by sonication for 30 min with a VCX-400 Vibracell (Sonics and Materials, Inc., Danbury, CT) operating at 20 kHz. The schematic diagram of preparation of S-INP is shown in Fig. 1. Morphological analysis of S-INP samples were performed by field emission scanning electron

**Fig. 1** Schematic diagram of the mechanism of INP stabilization by non-ionic surfactants

microscopy (FE-SEM). The specific surface area (S_{BET}) of the porous media, INP, and S-INP were measured by the Brunauer-Emmett-Teller (BET) N₂ method. X-ray photoelectron spectroscopy (XPS) was performed on INP and S-INP materials using a Physical Electronics 5500/5600 ESCA system. The mineralogy of INP, S-INP, and porous media was characterized by powder X-ray diffraction (XRD). Details about analytical methods are similar to that discussed in previous reports (Kanel et al. 2005, 2006).

Experimental setup

Pyrex glass columns of two lengths (10 cm × 2.5 cm internal diameter (ID) and 50 cm × 6 cm ID) were packed with porous media for the transport experiments. A porous glass diffuser plate placed on each end cap provided an even distribution of S-INP in the sand column and a nylon membrane capillary barrier was sealed at the bottom of each column. At the start of each experiment 10 pore volumes of DI water was passed through columns to enhance packing homogeneity. Influent solution flow rate was controlled with a peristaltic pump (Masterflex No.7553-85, Cole Parmer Instrument Company, USA). All column experiments were performed in triplicate and the S-INP elution data are expressed as the mean ± standard deviation of three replicate runs. Representative physical properties of packed 10 cm columns are presented in Table 2. Typical physical properties of a sand-packed 50 cm column were as follows: porosity: 0.58, bulk density: 1.5 g/cm³, organic matter content: 0.12%, surface area of sand: 0.64 m²/g and particle size: 425–600 μm.

Influent solutions containing 1 g L⁻¹ suspended S-INP with 0.5% surfactant in 0.01 M NaCl at pH 7 were prepared freshly prior to each column experiment. Columns were pretreated with S-INP

feed solution at a flow rate of 3 mL min^{-1} to the top of columns and column effluent was collected at desired time intervals with an auto fraction collector. About 2.4 L of 1 g L^{-1} S-INP suspension was typically required to reach S-INP breakthrough conditions in sand packed columns. Total Fe (particulate + dissolved) was measured by addition of 5 M HCl to effluent aliquots to dissolve particulate INP followed by reduction of Fe(III) to Fe(II) with hydroxylamine. Total dissolved Fe (as Fe(II)) was then determined using the phenanthroline colorimetric method with a Fe(II) detection limit of $4 \text{ }\mu\text{g/L}$ (Schrick et al., 2004; Leupin and Hug 2005). Total Fe was confirmed by flame atomic absorption spectrometry using a Perkin Elmer 5100 AAS. Soil organic matter (SOM) content and LOI were measured according to previous reports (Choi et al. 2002).

A stock solution of 1000 mg L^{-1} As(III) was prepared by dissolving NaAsO_2 in DI water followed by preparation of 200, 500 and $1000 \text{ }\mu\text{g L}^{-1}$ As(III) solutions in 0.01 M NaNO_3 . The pH of each solution was adjusted to 7.0 using 1 M NaOH or HCl . After achieving S-INP breakthrough, columns retained on average a total of $\sim 2 \text{ g S-INP}$. The As(III) influent solutions were pumped upward through S-INP pretreated columns at 1.8 mL min^{-1} flow rate. Effluent solutions were centrifuged and the supernatant solutions filtered ($0.45 \text{ }\mu\text{m}$) and total dissolved As was analyzed by hydride generation atomic absorption spectrophotometry (HGAAS; Perkin-Elmer 5100 PC). All experiments were performed in triplicate and data are expressed as the mean \pm standard deviation of three replicate runs.

Results and discussion

Characterization of INP and S-INP

Synthesis of INP by chemical precipitation (Kanel et al. 2005, 2006) followed by sonication in the presence of non-ionic surfactant (Tween-20) was employed in a similar technique as that of carbon nanotubes dispersion (Nepal and Geckeler 2006). This technique resulted in highly dispersible surface modified-INP (S-INP) in the aqueous phase. This was possible due to the association of

the hydrophobic part of the surfactant with the INP and the orientation of the hydrophilic part to the aqueous phase (Pileni 2003). On the other hand, pristine INP precipitated rapidly in approximately one minute (Fig. 2 inset a) whereas S-INP remained in dispersed form for a day (Fig. 2 inset b). Fig. 2 also shows the UV-Vis spectra of the surfactant, INP, and S-INP products in the aqueous phase. The surfactant has an absorbance peak at 234.5 nm and no detectable absorbance above 300 nm . Surfactant binding to INP causes a red shift to 236.5 nm plus a new peak appears at 263.5 nm . These peaks are effectively absent in pristine INP. A broadened peak at 346 nm ascribed to INP is seen clearly in both INP and S-INP spectra. These results indicate the successful dispersion of INP in aqueous surfactant solution. Results of XRD analysis (Fig. 2 inset) showed crystalline Fe^0 present in INP though surfactant modification of INP caused some peak broadening. We suspect that this is not due to amorphous Fe^0 but rather an artifact due to the surfactant coating.

The SEM images of pristine INP and S-INP are shown in Fig. 3. The image of pristine INP (Fig. 3a) shows rounded individual particles ranging in size from 10 to 160 nm . The INP particles ranging in sizes from 10 – 40 nm diameters are aggregated in chain like structures due to magnetic properties and the tendency to remain in the most thermodynamically favorable state (Cushing et al. 2004). In contrast the S-INP are dispersed and fully coated with the surfactant (Fig. 3b). S-INP observed by HR-TEM reveals a group of 10 – 40 nanoparticles of 2 – 10 nm diameter with a slight separation in between (Fig. 4b), possibly due to surfactant coating. The poor image contrast in Fig. 4b when compared to that of pristine INP (Fig. 4a) also resulted from the surfactant coating. Results from BET surface area analysis confirmed that S-INP surface area increased nearly three fold from $24.4 \text{ m}^2 \text{ g}^{-1}$ for pristine INP to $64.3 \text{ m}^2 \text{ g}^{-1}$ for S-INP.

XPS analysis of INP and S-INP surfaces provided the $\text{Fe } 2\text{p}^{3/2}$ and $\text{Fe } 2\text{p}^{1/2}$ photoemission spectra shown in Fig. 5. The two major peaks for $\text{Fe } 2\text{p}^{3/2}$ and $\text{Fe } 2\text{p}^{1/2}$ are at 710 and 724 eV , respectively and are assigned to the Fe^{3+} oxidation state whereas small peaks at 707 and 720 eV

Fig. 2 UV-VIS spectra of surfactant, INP and S-INP. Inset shows vials containing INP (a) and S-INP (b) and XRD of INP and S-INP

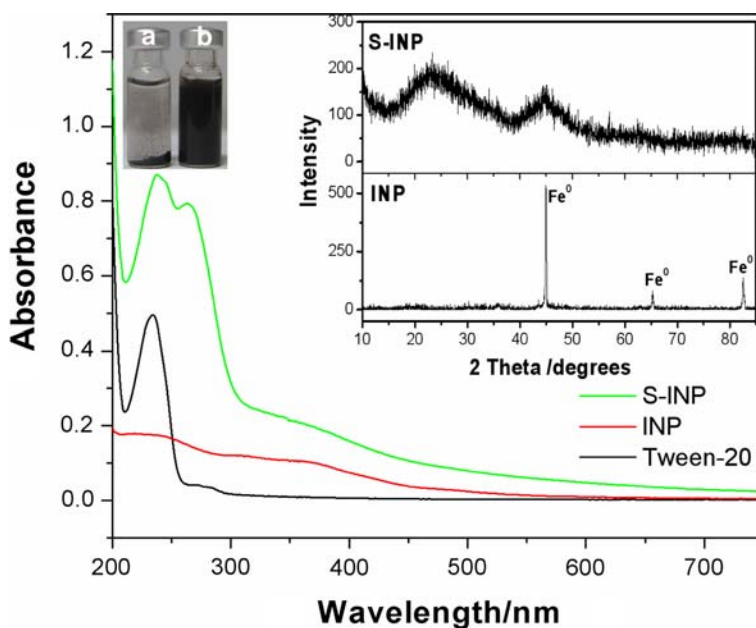
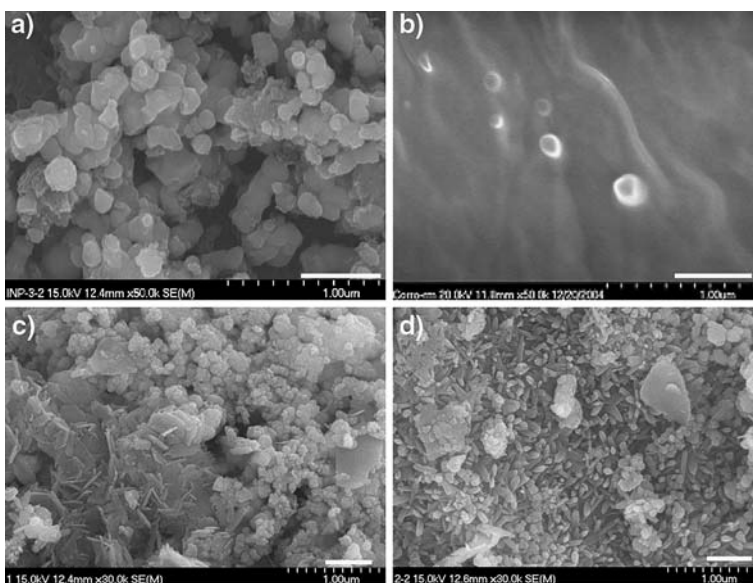


Fig. 3 SEM images of (a) INP and (b) S-INP (c) S-INP attached to sand during column experiment and (d) S-INP attached to sand after As(III) treatment. Scale bar represents 500 nm



are ascribed to the Fe^0 oxidation state (Nurmi et al. 2005; Fiedor et al. 1998). Our S-INP XPS data are nearly identical to those reported by Nurmi et al. (2005), who investigated air-exposed INP synthesized from H_2 gas and NaBH_4 reduction of Fe^{2+} . XPS is sensitive to the outer ~3–10 nm of the sample surface (Fiedor et al. 1998) and the presence of 707 and 720 eV peaks

suggests that the bulk of INP is Fe^0 covered with an oxidized Fe(III) layer. A slight reduction from 9.8 to 7.6% in the Fe^0 peak was observed after conversion of INP to S-INP as determined by curve fitting (Fig. 5). Generally it is presumed that % Fe^0 would be reduced after sonication due to production of OH radical, which would oxidize Fe^0 to Fe(III) (Dai et al. 2006).

Fig. 4 HR-TEM images of pristine INP (a) and S-INP (b)

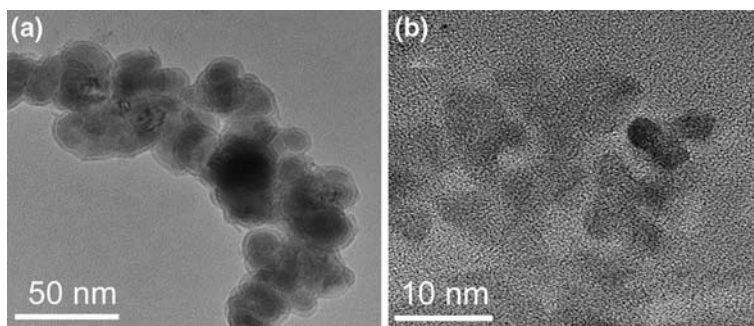
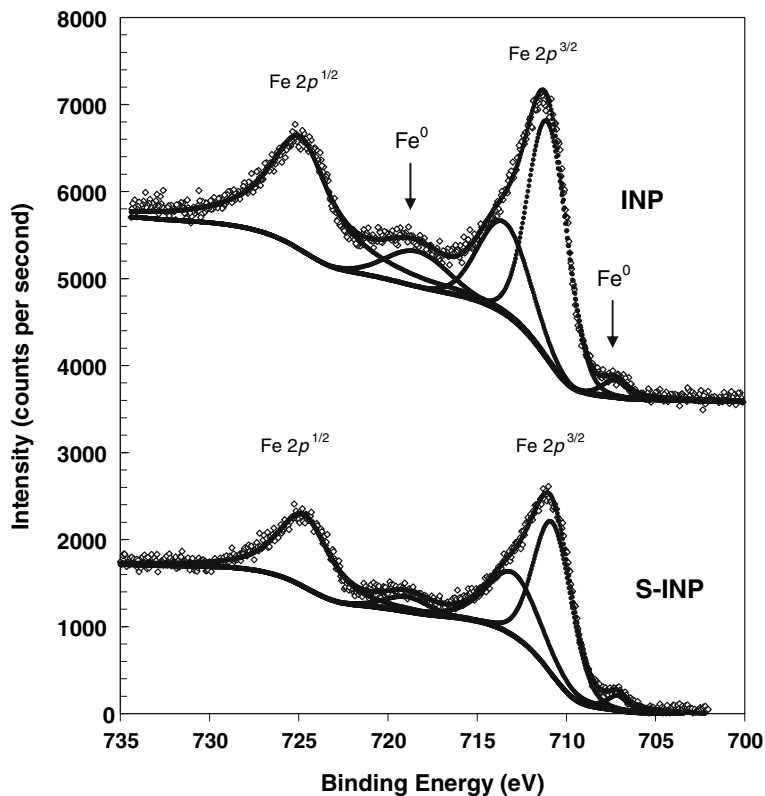


Fig. 5 Fe 2p XPS analysis of pristine INP and S-INP. Points are experimental data and lines are Gaussian peak fits

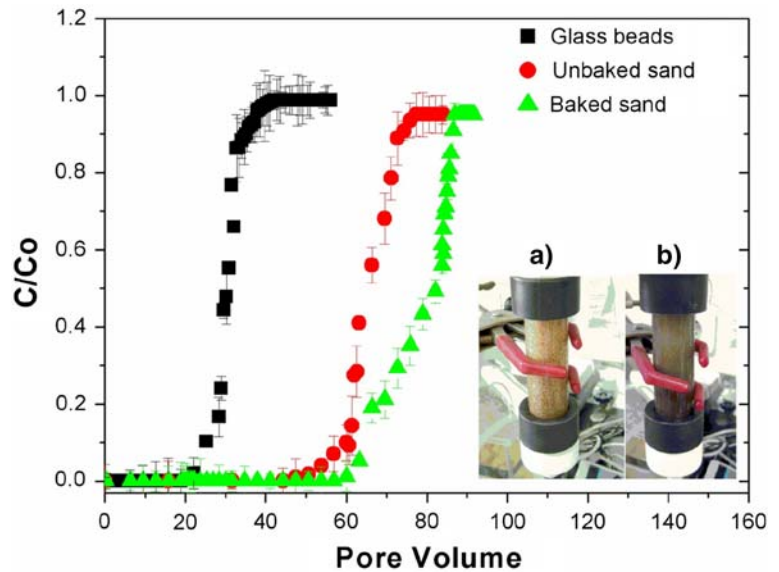


Transport of INP and S-INP in porous media

The dramatic difference in the transport of unmodified INP and S-INP is illustrated in Fig. 8 (inset). When unmodified INP was introduced to the top of a sand packed column, particle aggregation occurred inhibiting downward transport (Fig. 8 inset a). The 50 cm columns were used for the demonstration of S-INP transport (Fig. 8 inset) and long term studies whereas 10 cm columns (Fig. 6b inset) were used in all other experiments.

Figure 6 shows S-INP break through curves (BTC) from sand-packed columns (Fig. 6 inset) maintained at water saturation of 30%. The S-INP feed solution was injected through columns downward at a rate of 3 mL/min using a peristaltic pump until a constant effluent S-INP concentration was reached. For glass beads, unbaked sand and baked sand, 22.1, 47.4 and 60.1 pore volumes were required to reach this condition, respectively. Glass beads allowed S-INP to migrate with little surface interaction whereas the sand contained small quantities of Al and Fe metal oxides (MO)

Fig. 6 Breakthrough curves of S-INP in glass beads, unbaked sand, and baked sand packed in 10 cm columns; S-INP concentration 1 g/L, surfactant: 0.5%, flow rate: 3.0 ml/min in downward direction. Inset shows short columns (10 cm length) used for the experiments before passing S-INP (a) and after passing S-INP (b)



and 0.12% soil organic matter (SOM) (Table 1) causing retardation of S-INP breakthrough. The increased S-INP breakthrough volume in baked sand suggested that the baking process caused formation of active surface sites with increased affinity for S-INP. After passing through the sand packed column the S-INP morphology indicated corrosion to Fe(III) hydroxide had occurred (Fig. 3c) along with significant aggregation due to dissolution of surfactant.

The attachment coefficient, α , for S-INP in glass beads, sand, and baked sand was calculated from observations of C/C_0 in 10-cm using following equations (Schrick et al. 2004; Elimelech 1994; Yao et al. 1971).

$$\alpha = \frac{2d_c}{3(1-f)L\eta_0} \ln(C/C_0) \tag{1}$$

where d_c is the diameter of a collector (assumed to be spherical) in the porous medium, f is the porosity of the porous medium, L is the length of the porous medium, C and C_0 are the particle concentrations present at distance L and at $L = 0$, respectively and η_0 is the clean bed single collector efficiency that describes the particle transport to an individual collector. The clean bed collector efficiency can be calculated as function of the Darcy velocity, porous medium grain size, porosity, and temperature among other variables (Rajagopalan and Tien 1976; Tufenkji

and Elimelech 2004). The attachment efficiency, α , may be treated as an empirical parameter that captures all aspects of particle deposition not described by the more extensively validated particle transport models (Yao et al. 1971). Using equation 1 and Fig. 6 we obtained α values of 0.01, 0.21 and 0.18 for glass beads, unbaked sand and baked sand, respectively (Table 3). Schrick et al. (2004) reported similar α values for polyacrylic acid coated zero-valent INP as 0.36 for Ottawa sand.

Removal of Arsenic(III) by S-INP

In situ remediation of As(III) was investigated in S-INP pre-treated 10 cm columns (Fig. 7). After S-INP breakthrough the sand packed column retained ~2 g of S-INP. Complete As(III) removal was observed up to 9, 8, 4 days for 200, 500, 1000 $\mu\text{g L}^{-1}$ of initial As(III) concentration, respectively (Fig. 7). Our preliminary studies suggested that As(III) was not adsorbed strongly by the untreated porous media. The resulting As loading on the S-INP-treated sand columns at breakthrough was 2.3, 5.2 and 5.2 mg g^{-1} providing 23.3 L, 20.7 L and 10.4 L of arsenic free water for the 200, 500, 1000 $\mu\text{g L}^{-1}$ influent As(III) concentrations, respectively. Recently, Leupin and Hug (2005) studied a prototype zero-valent iron (ZVI) column for the removal of As from Bangladesh well water. Up to 36 L of well water

Table 3 S-INP Attachment Efficiency in Porous Media packed in short columns (10 cm length)

Porous Media	α	η	C/C_0
Glass Bead	0.01	0.012	0.98
Unbaked Sand	0.21	0.009	0.80
Baked Sand	0.18	0.009	0.80

Where, α : the attachment coefficient, η : collector efficiency and C/C_0 : ratio of effluent and initial concentration of total iron. Error estimates for calculated α values based on three replicates was $< \pm 10\%$.

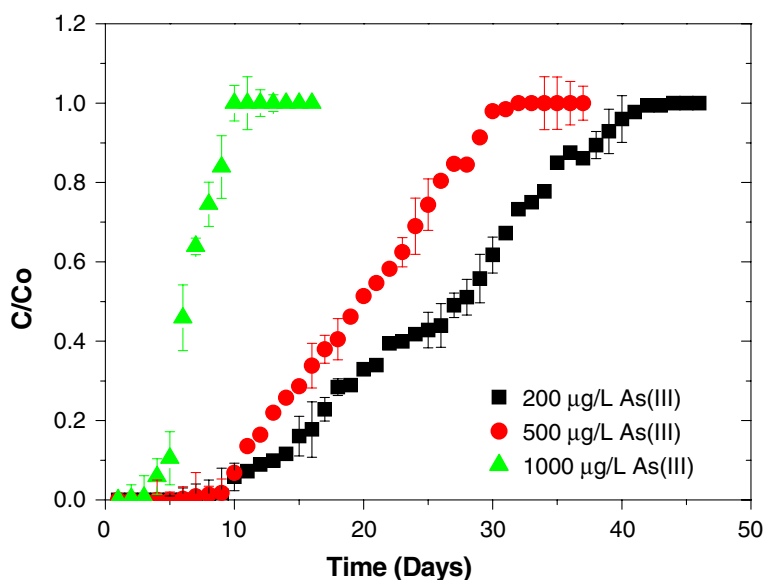
containing $440 \mu\text{g L}^{-1}$ was effectively treated with a succession of four ZVI/sand filters containing 1.5 g micron size ZVI and 60 g sand to below $50 \mu\text{g L}^{-1}$ resulting in As loading on ZVI of 2.64 mg g^{-1} . In the current study, it was observed that $\sim 30 \text{ L}$ of $500 \mu\text{g/L}$ of As(III) was treated to undetectable levels using $\sim 2 \text{ g}$ S-INP continuously without changing the S-INP resulting in As loading on INP of 5.2 mg g^{-1} .

Arsenic(III) adsorption on S-INP occurs on a short time scale (minutes) to form strong adsorption complexes. The adsorption of As(III) and As(V) on ZVI powders has been previously investigated with EXAFS spectroscopy and results of these investigations suggest that adsorption sites are formed by formation of either a mixed Fe(II)/(III) or Fe(III) oxide, hydroxide, or oxyhydroxide corrosion products (Manning et al. 2002; Farrell et al. 2001). The presence of the

surfactant molecule in S-INP may affect the crystallinity of the Fe oxide/hydroxide products formed during corrosion. Our XRD results for reacted S-INP did not show a crystalline Fe corrosion product phase (data not shown). However, it is possible that over longer periods slow formation of crystalline products such as Fe(II)/(III) oxides (magnetite, maghemite), ferric hydroxides (ferrihydrite), and Fe(III) oxyhydroxides (goethite and lepidocrocite) occurs.

Recently it has been shown that As(III) is oxidized to As(V) during the corrosion of metallic Fe (Leupin and Hug 2005; Manning et al. 2002; Su and Puls 2001). Both As(III) and As(V) are adsorbed by formation of strong inner sphere surface complexes on Fe(III) oxides/hydroxides (Manning et al. 2002; Farrell et al. 2001; Manning et al. 1998). Layers of As(III) and As(V) adsorbed on INP corrosion product films are buried by successive Fe(III) oxides/hydroxide layers and become occluded from the surrounding solution. For this reason we suspect that As(III) oxidation would occur in the presence of the corroding INP (Kanel et al. 2005) and S-INP surfaces and that adsorption occurred via inner sphere surface complexation. The morphology of S-INP was also altered in the presence of As(III) (Fig. 3d), which resulted in separated and elongated, rod-like shaped particles which were X-ray amorphous (data not shown).

Fig. 7 Breakthrough curves of As(III) (200, 500 and $1000 \mu\text{g/L}$) passed through S-INP (2.0 g) anchored on sand (425–600 μm) packed columns; flow rate: 1.8 ml/min in upward direction



Long-term study

Long term experiments using 50 cm columns (see Fig. 8 photo inset) were conducted to study the effectiveness of S-INP as a colloidal reactive barrier for groundwater aquifer treatment. S-INP suspension was passed through the column at the rate of 3 mL/min in a downward direction until the S-INP eluted from the column (Fig. 8b inset). After anchoring S-INP (~12 g per column) As(III), solution was introduced in the upward direction at a flow rate of 1.8 mL/min. Under these column and flow conditions, As(III) was completely removed for about 3 month providing 194.4 L of arsenic free water. The S-INP was corroded to magnetite and remained in the sand packed column for more than 10 months. Overall, the state of S-INP suggested that it could be used as mobile-colloidal reactive barrier (M-CRB) for *in-situ* deep groundwater aquifer treatment.

Comparison of surface modified INP for removal of different contaminants

Table 4 was compiled to compare the results of different environmental applications of S-INP. It is clearly seen from the Table 4 that the surface area was highest (64.3 m²/g) for Tween 20 stabilized S-INP. Although no previous studies have investigated removal of dissolved As using S-INP,

remediation of organic contaminants such as TCE has been demonstrated with S-INP using different stabilizers. For example, He and Zhao (2005) used a batch approach to treat TCE using starch stabilized INP. Schrick et al. (2004) studied transport of surface modified INP using PAA and carbon in a burette filled with sand or soil. Though transport of S-INP was demonstrated, and removal of TCE was successfully shown in batch experiments, application to removal of pollutants in columns was not shown. Similarly, Elliott and Zhang (2001) reported batch and field study of palladium stabilized INP and their reactivity with TCE. Quinn et al. (2005) demonstrated dense non-aqueous phase liquid (DNAPL) remediation using an oil/surfactant INP emulsion in field scale. Our results demonstrate that natural sand pretreated with S-INP is an effective barrier for As(III) removal and may be applicable to certain sandy ground water aquifer field conditions. The S-INP material may also be used for remediation of other pollutants such as TCE, PCE and PAHs without excavation of soil.

Conclusions

The synthetic S-INP used in this study had a particle size range from 2 to 10 nm. Though XRD

Fig. 8 Breakthrough curves of As(III) (500 µg/L) passed through S-INP (12 g) anchored sand (425–600 µm) packed columns; flow rate: 1.8 ml/min in upward direction (a) and Column showing S-INP passing through sand packed column. Inset shows comparison of effluents collected without surfactant (INP) (a) & with surfactant (S-INP) (b), an arrow in (a) shows INP stuck at the top

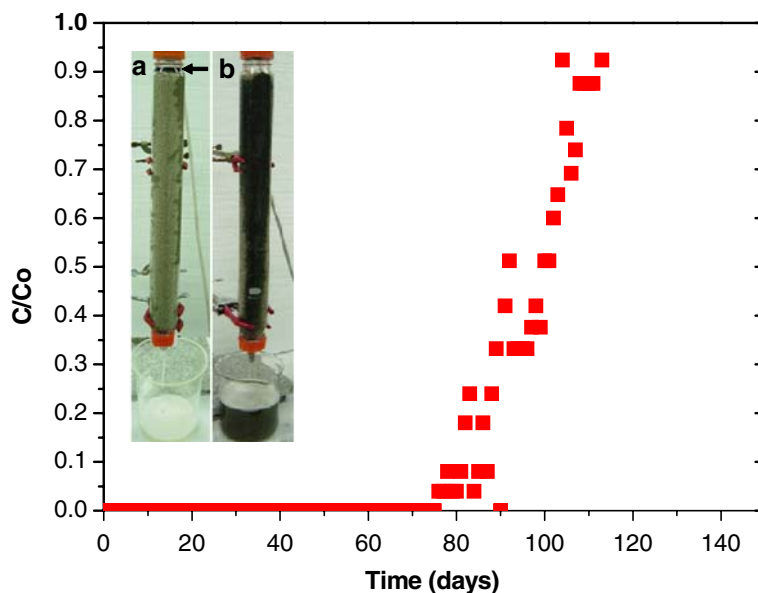


Table 4 Comparison of properties and application of surface modified INP using different stabilizers

Stabilizer	Experimental condition	BET-area (m ² /g)	Particle Size (nm)	Results	Ref.
PAA ^a	Transport tested in burette packed with soil and sand, and applied to remove TCE (batch)	20–30	20–30	40% of TCE (13ppm) was removed by 0.016 g of PAA-INP	Schrick et al. (2004)
Starch	Batch study to remove TCE	55	55	98% TCE (25 ppm) was removed by 1 g/L starch-INP in 1 h	He and Zhao (2005)
Metal (Pd) ^b	Batch and field study to remove TCE	–	100–200	96% TCE was removed	Elliott and Zhang (2001)
Emulsion ^c	Applied in field to remove TCE	–	–	57–100% TCE was removed in targeted sited	Quinn et al. (2005)
Tween 20	Column study with natural sand packed column to remove As(III).	64	2–10	100% As (0.2 ppm) was removed by the 10 cm column for 9 days whereas in 50 cm column 100% of 0.5 mg/L of As(III) was removed for 90days	This study

^a Poly acrylic acid, ^b INP was coated by palladium (Pd), which help to stabilize and mobile in soil, ^c emulsion was prepared by mixing oil surfactant (span 85) and water

showed crystalline Fe⁰ was present, XPS analysis confirmed that an oxidized surface layer was present on these particles. Surface modification by surfactant resulted in fully dispersed S-INP in aqueous solution that was mobile in a sand-packed column. In this study we have shown that 0.2 mg L⁻¹ As(III), a concentration that is 20 × greater than the current safe drinking water standard, is removed by S-INP pretreated sand for more than 9 days in 10 cm columns containing ~2 g total iron providing 23.3 L of arsenic free water. The As(III) is strongly adsorbed on S-INP corrosion products at neutral pH. In applications using 50 cm length columns, dissolved As(III) solution (0.5 mg/L) flowing at 1.8 mL/min was 100% removed for more than 2.5 months providing 194.4 L of arsenic free water. Our work demonstrates that surfactant modification is an effective treatment to enhance the transport of INP through porous media, which suggests that S-INP has great potential to be applied by slurry injection to a targeted subsurface site from the surface in areas where excavation is difficult.

Acknowledgements This work was supported by a grant from the National Research Laboratory Program by the Korea Science and Engineering Foundation. This work

was also supported by a Research Corporation Cottrell College Science Award grant (CC5444).

References

- Choe S, Chang YY, Hwang KY, Khim J (2000) Kinetics of reductive denitrification by nanoscale zero-valent iron. *Chemosphere* 41(8):1307–1311
- Choi H, Lim H, Kim J, Hwang T, Kang J (2002) Transport characteristics of gas phase ozone in unsaturated porous media for in-situ chemical oxidation. *J Cont Hydro* 57(1–2):81–98
- Cushing BL, Kolesnichenko VL, O'Connor CJ (2004) Recent advances in the liquid-phase syntheses of inorganic nanoparticles. *Chem Rev* 104(9):3893–3946
- Dai Y, Li F, Ge F, Zhu F, Wu L, Yang X (2006) Mechanism of the enhanced degradation of pentachlorophenol by ultrasound in the presence of elemental iron. *J Haz Mat* 137(3):1424–1429
- Elimelech M (1994) Effect of particle size on the kinetics of particle deposition under attractive double layer interactions. *J Col Interf Sci* 164(1):190–199
- Elliott DW, Zhang W-X (2001) Field assessment of nanoscale bimetallic particles for groundwater treatment. *Environ Sci Technol* 35(24):4922–4926
- Farrell J, Wang J, O'Day P, Coklin M (2001) Electrochemical and spectroscopic study of arsenate removal from water using zero-valent iron media. *Environ Sci Technol* 35(10):2026–2032
- Ferguson JF, Gavis J (1972) Review of the arsenic cycle in natural waters. *Water Res* 6(11):1259–1274

- Fiedor JN, Bostick WD, Jarabek RJ, Farrell J (1998) Understanding the mechanism of uranium removal from groundwater by zero-valent iron using x-ray photoelectron spectroscopy. *Environ Sci Technol* 32(10):1466–1473
- He F, Zhao D (2005) Preparation and characterization of a new class of starch-stabilized bimetallic nanoparticles for degradation of chlorinated hydrocarbons in water. *Environ Sci Technol* 39(9):3314–3320
- Huber DL (2005) Synthesis, properties, and applications of iron nanoparticles. *Small* 1(5):482–501
- Joo SH, Feitz AJ, Waite TD (2004) Oxidative degradation of the carbothioate herbicide, molinate, using nanoscale zero-valent iron. *Environ Sci Technol* 38(7):2242–2247
- Kanel SR, Grenèche JM, Choi H (2006) Arsenic (V) removal from groundwater using nano scale zero-valent iron as a colloidal reactive barrier material. *Environ Sci Technol* 40(6):2045–2050
- Kanel SR, Manning B, Charlet L, Choi H (2005) Removal of Arsenic(III) from groundwater by nanoscale zero-valent iron. *Environ Sci Technol* 39(5):1291–1298
- Kanel SR, Neppolian B, Choi H, Yang JW (2003) Heterogeneous catalytic oxidation of phenanthrene by hydrogen peroxide in soil slurry: kinetics, mechanism and implication. *Soil and Sediment Contamination* 12(1):101–117
- Leupin OX, Hug SJ (2005) Oxidation and removal of arsenic (III) from aerated groundwater by filtration through sand and zero-valent iron. *Water Res* 39(9):1729–1740
- Li L, Fan M, Brown RC, Leeuwen JV, Wang J, Wang W, Song Y, Zhang P (2006) Synthesis, properties and environmental applications of nanoscale iron-based materials: A review. *Crit Rev Environ Sci Technol* 36(5):405–431
- Lowry GV, Johnson KM (2004) Congener-Specific Dechlorination of Dissolved PCBs by Microscale and Nanoscale Zerovalent Iron in a Water/Methanol Solution. *Environ Sci Technol* 38 (19):5208–5216
- Manning BA, Fendorf SE, Goldberg S (1998) Surface structures and stability of arsenic(III) on goethite: Spectroscopic evidence for inner-sphere complexes. *Environ Sci Technol* 32(16):2383–2388
- Manning BA, Hunt M, Amrhein C, Yarmoff JA (2002) Arsenic(III) and Arsenic(V) reactions with zerovalent iron corrosion products. *Environ Sci Technol* 36(24):5455–5461
- Nepal D, Geckeler KE (2006) pH-sensitive dispersion and debundling of single-walled carbon nanotubes: Lysozyme as a tool. *Small* 2(3):406–412
- Nurmi JT, Tratnyek PG, Sarathy V, Baer DR, Amonette JE, Pecher K, Wang C, Linehan JC, Matson DW, Penn RL, Driessen MD (2005) Characterization and properties of metallic iron nanoparticles: Spectroscopy, electrochemistry, and kinetics. *Environ Sci Technol* 39(5):1221–1230
- O'Hena S, Krug T, Quinn J, Clausen C, Geiger C (2006) Field and laboratory evaluation of the treatment of DNAPL source zones using emulsified zero-valent iron. *Remediation* 16(2):35–56
- Pileni M-P (2003) The role of soft colloidal templates in controlling the size and shape of inorganic nanocrystals. *Nat Mat* 2(3):145–150
- Ponder SM, Darab JC, Mallouk TE (2000) Remediation of Cr(VI) and Pb(II) aqueous solutions using supported, nanoscale zero-valent iron. *Environ Sci Technol* 34(12):2564–2569
- Quinn J, Geiger C, Clausen C, Brooks K, Coon C, O'Hara S, Krug T, Major D, Yoon W-S, Gavaskar A, Holdsworth T (2005) Field demonstration of DNAPL dehalogenation using emulsified zero-valent iron. *Environ Sci Technol* 39(5):1309–1318
- Rajagopalan R, Tien C (1976) Trajectory analysis of deep-bed filtration with sphere-in-cell porous-media model. *AIChE J* 22(3):523–533
- Schrick B, Hydutsky BW, Blough JL, Mallouk TE (2004) Delivery vehicles for zerovalent metal nanoparticles in soil and groundwater. *Chem Mater* 16(11):2187–2193
- Su C, Puls RW (2001) Arsenate and arsenite removal by zerovalent iron: Kinetics, redox transformation, and implications for in situ groundwater remediation. *Environ Sci Technol* 35(7):1487–1492
- Tufenkji N, Elimelech M (2004) Correlation equation for predicting single-collector efficiency in physicochemical filtration on saturated porous media. *Environ Sci Technol* 38(2):529–536
- Wang CB, Zhang W (1997a) Synthesizing nanoscale iron particles for rapid and complete dechlorination of TCE and PCBs. *Environ Sci Technol* 31 (7):2154–2156
- Yao KM, Habibian MT, O'Melia CR (1971) Water and waste water filtration: concepts and applications. *Environ Sci Technol* 5(11):1105–1112
- Zhang WX (2003) Nano scale iron particles for environmental remediation: an overview. *J Nanoparticle Res* 5(3–4):323–332